

CoFe stripes: Magnetization reversal study by polarized neutron scattering and magneto-optical Kerr effect

Katharina Theis-Bröhl,* Till Schmitte, Vincent Leiner, and Hartmut Zabel

Institute für Experimentalphysik / Festkörperphysik, Ruhr-Universität Bochum, 44780 Bochum, Germany

Karsten Rott and Hubert Brückl

Department of Physics, Universität Bielefeld, Universitätsstrasse 25, 33615 Bielefeld, Germany

Jeffery McCord

Institut für Festkörperforschung, Helmholtzstrasse 20, 01169 Dresden, Germany

(Received 15 August 2002; published 23 May 2003)

We have studied the magnetization reversal of a laterally structured film with both, magneto-optical Kerr effect and with polarized neutron scattering in the off-specular regime. The lateral structure consists of 90-nm thick and 1.2- μm wide $\text{Co}_{0.7}\text{Fe}_{0.3}$ stripes with a grating period of 3 μm . Magnetization reversals were measured for different orientations of the sample with respect to the field directions. In addition, Kerr microscopy was used for visualizing the domain state. Due to the high aspect ratio of the individual stripes, the remagnetization process of the stripe array is dominated by a single domain state over most of the field range. For the easy axis direction, a nucleation and domain wall movement is observed at the coercive field. However, for all other orientations of the stripe array the magnetization reversal is dominated by a coherent magnetization rotation up to the coercive field. For the hard axis orientation the coherent rotation is complete. For this particular stripe array, the agreement between results obtained from MOKE and PNS experiments is very good, mainly due to the specific sample design chosen.

DOI: 10.1103/PhysRevB.67.184415

PACS number(s): 75.60.Ej, 75.75.+a, 61.12.Ha

I. INTRODUCTION

Microstructured and nanostructured samples have created much interest in recent years because of their potential applications in optical and magnetic storage devices. In particular, the magnetic properties of periodic arrays of micron and submicron size dots¹⁻⁶ and stripes⁷⁻¹¹ have attracted much attention recently. A number of methods have been applied to characterize the magnetic properties of these patterns, including the magneto-optical Kerr effect (MOKE),¹²⁻¹⁴ Kerr microscopy,¹⁵ scanning electron microscopy with polarization analysis (SEMPA),¹⁶ Lorentz microscopy,¹⁷ x-ray magnetic circular dichroism (XMCD) microscopy,¹⁸ and magnetic force microscopy (MFM).¹⁹ In comparison, neutron scattering has rarely been applied to patterned structures, although the interpretation of neutron data is more straightforward than for most other methods. Clearly, the disadvantage of neutron scattering is the low intensity from a tiny scattering volume resulting in long counting times. Nevertheless, applying polarized neutron-scattering methods to micrometer and submicrometer scale lateral structures is a new and challenging task, which can yield new insight into the analysis of the remagnetization processes. There are only few examples reported so far of successful neutron-scattering experiments on laterally structured magnetic arrays. Polarized neutron-scattering (PNS) maps from magnetic dot arrays have been measured in remanence by Toperverg *et al.*²⁰ and the magnetization reversal of magnetic dots and bars with pronounced dipole character was recently investigated via PNS by Temst *et al.*^{21,22} However, a critical comparison between MOKE and PNS results from stripe arrays is missing so far.

In this paper we present a comparative MOKE and PNS

study to determine the magnetic hysteresis of a periodic magnetic stripe array. For homogeneous magnetic films, both the vector MOKE and the polarized specular neutron reflectivity (PNR) yield the in-plane magnetization vector, and, in general, good agreement is found between both the methods.²³⁻²⁵ Deviations may arise from differences in the sampling volume and the averaging procedure over different magnetic domains. The advantage of PNR over MOKE is that the former method has a higher penetration depth and simultaneously yields structural information, allowing a layer resolved vector magnetometry of several magnetic layers stacked on top of each other.

We used CoFe stripes of 1.2 μm width forming an array with a lattice parameter of 3 μm . The magnetization reversal process was investigated for different sample orientations with respect to the scattering plane, i.e., at different angles of the stripe orientation with respect to the applied magnetic field. We performed measurements in the off-specular scattering regime along the q_x direction, i.e., magnetization reversal studies at the first-order Bragg peak of the lateral structure projected into the scattering plane. The polarized neutron data are compared to MOKE measurements taken in longitudinal geometry. In addition, MOKE measurements with a transverse magnetic field were performed, resulting in hysteresis loops of the transverse magnetization component. This allows us to use a vector model for the magnetization process as has been shown by Daboo *et al.*²⁶

For the case of magnetic stripe arrays, the comparison between MOKE and polarized neutron scattering is not as straightforward as for homogeneous films, since we will compare vector-MOKE results with polarized neutron scattering from the first-order Bragg peaks of the stripe pattern at

small angles. In this configuration, neutron scattering promises to be sensitive to correlation effects during the remagnetization of the individual stripes, which are much more difficult to access with other methods. Correlation effects can, in principle, also be analyzed with MOKE, when the hysteresis is measured in higher order of the interference pattern. In the past, we have demonstrated the usefulness of the longitudinal Bragg-MOKE method for the analysis of magnetic stripe arrays.^{12–14} On the other hand, the Bragg MOKE does not allow a vector magnetometry. Only the combination of Bragg MOKE and vector MOKE would be equivalent to polarized neutron scattering, which, however, has not been realized up to now. Therefore, in the present study we will compare vector MOKE with PNS.

Two experimental difficulties have to be overcome to successfully use neutron-scattering techniques for magnetic stripe arrays: first a large and homogeneously structured sample area is required and second unfavorable scattering vectors often need to be probed from arrays patterned on a micrometer and submicrometer scale. In the following section we will discuss and explain how to cope with these difficulties.

This paper is organized as follows. We first describe in Sec. II, the methods for producing an array of magnetic stripes and the experimental techniques used for analyzing their magnetization reversal. In Sec. III, we discuss the results obtained with different methods, and in Sec. IV we compare the MOKE and the neutron results. In Sec. V, we summarize our results.

II. EXPERIMENTAL DETAILS

A. Sample preparation

The sample studied in this paper is a $20 \times 10 \text{ mm}^2$ $\text{Co}_{0.7}\text{Fe}_{0.3}$ thin polycrystalline film grown by dc magnetron sputtering. For the present study a polycrystalline film is preferred to average the intrinsic magnetocrystalline anisotropy. The films have no further intentionally induced anisotropy, such that their anisotropy is dominated by the shape anisotropy. CoFe films with the quoted composition have been shown to exhibit the largest tunneling magnetoresistance²⁷ and have been introduced as electrodes in magnetic tunnel junctions for magnetoelectronic devices.²⁸ We used $\text{Al}_2\text{O}_3(1\bar{1}02)$ as a substrate with a 5-nm thick Ta buffer layer. The sample was spin coated with Novolak photoresist, which was exposed by 442-nm light in a scanning laser lithography setup and developed afterwards. A layer stack consisting of 5 nm Ta, 90 nm $\text{Co}_{0.7}\text{Fe}_{0.3}$, and a 5-nm Ta protection layer was deposited onto the patterned photoresist. Finally, the photoresist was removed via liftoff. The described procedure resulted in $\text{Co}_{0.7}\text{Fe}_{0.3}$ stripes of $1.2 \mu\text{m}$ width and a grating parameter of $d=3 \mu\text{m}$ as can be seen from the AFM picture in Fig. 1.

B. MOKE measurements

Hysteresis loops were measured by using a high-resolution MOKE setup in the longitudinal configuration with *s*-polarized light, which is well suited for measuring the

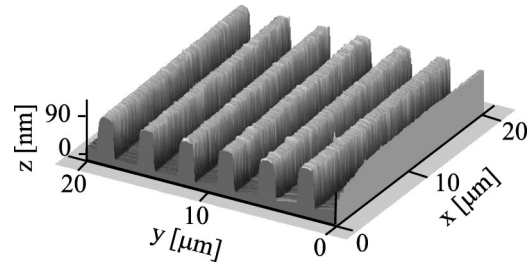


FIG. 1. Surface topography of the array of $\text{Co}_{0.7}\text{Fe}_{0.3}$ stripes obtained with an atomic force microscope shown in a three-dimensional surface view. The displayed area is $20 \times 20 \mu\text{m}^2$.

Kerr angle as a function of the applied magnetic field. More details of the experimental setup can be found in Ref. 29. In the longitudinal configuration, the magnetic field is directed along the plane of incidence and parallel to the sample surface. In this case, the measured Kerr angle is proportional to the component of the magnetization vector along the field direction, $\theta_K^l \propto m_L$, where m_L is the longitudinal component of \vec{M} in a projection parallel to \vec{H} . In addition, the experimental setup allows for a rotation of the sample around its surface normal (angle χ) in order to apply a magnetic field in various in-plane directions. Hysteresis measurements in the longitudinal configuration do not allow to distinguish directly between a magnetization reversal via domain rotation and/or via domain formation and wall motion. Therefore, we have also performed MOKE measurements with the external magnetic-field oriented perpendicular to the plane of incidence. In this so-called perpendicular configuration, the magneto-optical Kerr effect measures the magnetization component parallel to the plane of incidence but perpendicular to the applied magnetic field, $\theta_K^t \propto m_T$. Both components of the magnetization m_L and m_T yield the average magnetization vector \vec{M} as measured within the region illuminated by the laser spot ($\approx 1 \text{ mm}^2$). The experimental setup for these measurements is shown schematically in Fig. 2.

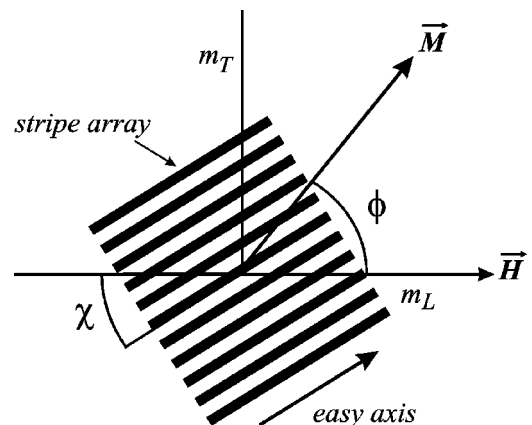


FIG. 2. Sketch of the longitudinal MOKE setup with the sample rotation angle χ between the easy axis and the applied field, and the angle ϕ of the magnetization vector \vec{M} . In the transverse configuration, the field and the sample are rotated by 90° , such that the angle χ is kept constant, but the magnetization component m_T is in the plane of incidence.

Assuming that the proportionality constant between θ_K and the components of \vec{M} is the same for both configurations, we may write

$$\frac{m_L}{m_T} = \frac{\cos \phi}{\sin \phi} = \frac{\theta_K^L}{\theta_K^T}, \quad (1)$$

from which follows the angle of rotation ϕ of the magnetization vector \vec{M} ,

$$\phi = \arctan\left(\frac{\theta_K^T}{\theta_K^L}\right). \quad (2)$$

Furthermore, we can express $|M|$, normalized to the saturation magnetization,

$$\frac{|M|}{|M|^{sat}} = \frac{\theta_K^L}{\theta_K^{L,sat}} \frac{1}{\cos \phi}. \quad (3)$$

For the MOKE experiment, the sample is first placed in the longitudinal configuration and hysteresis loops are measured for various in-plane rotation angles χ . The measurements are then repeated in the perpendicular configuration. For both configurations, $\chi=0^\circ$ is defined as the angle for which the external magnetic field is aligned parallel to the CoFe stripes (see Fig. 2). The parallel alignment is calibrated by using the interference pattern generated by diffraction of the laser beam at the grating. This procedure leads to an uncertainty in the definition of χ of less than $\pm 1^\circ$.

C. Kerr microscopy measurements

The imaging of the structures was performed by magneto-optical Kerr microscopy in the longitudinal mode.¹⁵ The weak magneto-optical contrast was digitally enhanced by means of a background subtraction technique.³⁰ The experimental setup has the option to apply in-plane magnetic fields in any direction independently of the magneto-optical sensitivity direction. To visualize the magnetic domains within the narrow stripes, the highest possible optical resolution, which is on the order of $0.3 \mu\text{m}$ for the given visible light illumination, was chosen.

D. Neutron-scattering experiments

Neutron-scattering experiments were performed at the ADAM reflectometer at the Institute Laue-Langevin in Grenoble, France. Measurements without and with spin polarization/analysis use a neutron wavelength of 0.441 nm . The scattering geometry is depicted in Fig. 3. For field-dependent measurements, an electromagnet was used with a field direction perpendicular to the scattering plane and parallel to the incident neutron polarization axis. The magnet reaches a maximum field of 2000 Oe at the sample position. Prior to each neutron measurement performed at zero field or at a constant field value, the sample was first saturated and then the field was reduced to the respective value, where it was kept constant during the measurement. For performing magnetization reversal measurements, the sample was first

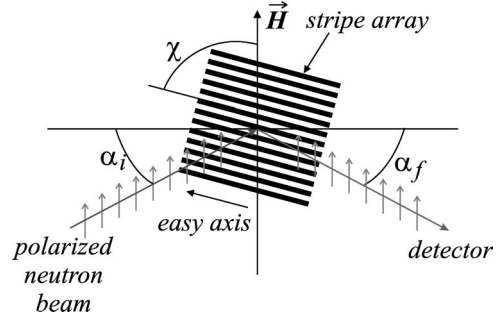


FIG. 3. Sketch of the neutron-scattering geometry. χ is the angle of the sample rotation with respect to the applied field (same definition as in Fig. 2). The magnetic field \vec{H} is applied perpendicular to the scattering plane. α_i and α_f refer to the incident and exit angles of the neutrons to the sample surface.

saturated in a field of -2000 Oe , applied perpendicular to the scattering plane and opposite to the neutron polarization axis. The first part of each magnetization reversal measurement was then carried out after returning to remanence in an increasing magnetic field between 0 and $+820 \text{ Oe}$. Subsequently, the sample was saturated at $+2000 \text{ Oe}$. In the second part of the measurement, the field was reduced and measurements were taken between $+720 \text{ Oe}$ and 0 . This procedure allows to measure the positive and negative branches of the magnetization curve while keeping the external field always in the same direction as the neutron guide field; a depolarization of the beam can thus be avoided.

From the four different cross sections measured at the specular reflection, one can determine the spin asymmetry as a function of external field $S_a(H)$:

$$S_a = \frac{I_+ - I_-}{I_+ + I_-} = \frac{I_{+,+} + I_{+,-} - I_{-,-} - I_{-,+}}{I_{+,+} + I_{+,-} + I_{-,-} + I_{-,+}}, \quad (4)$$

using the intensities of the non-spin-flip $[(+,+), (-,-)]$ and the spin-flip $[(+,-), (-,+)]$ cross sections. Due to the linear dependence of the magnetic part V_{mag} of the optical potential,

$$V = V_{nuc} \pm V_{mag} \quad (5)$$

to the magnetic induction \mathbf{B} , with $+$ for “up” neutrons and $-$ for “down” neutrons, the spin asymmetry shows a linear dependence on the magnetization in case of specular reflection. For the Bragg reflections, scattering theory has to be applied. Using kinematic scattering theory within the first Born approximation, S_a is not a simple function on the magnetization. In order to find a linear dependence, one can define an expression similar to the spin asymmetry:

$$S'_a = \frac{\sqrt{I_+} - \sqrt{I_-}}{\sqrt{I_+} + \sqrt{I_-}} = \frac{\sqrt{I_{+,+} + I_{+,-}} - \sqrt{I_{-,-} + I_{-,+}}}{\sqrt{I_{+,+} + I_{+,-}} + \sqrt{I_{-,-} + I_{-,+}}}, \quad (6)$$

with S'_a being proportional to the magnetization component along the y axis. It should, however, be kept in mind that this is only a rough approximation for the distorted Born wave approximation, which actually is to be applied when analyzing Bragg peaks close to the Yoneda wings. Assuming the

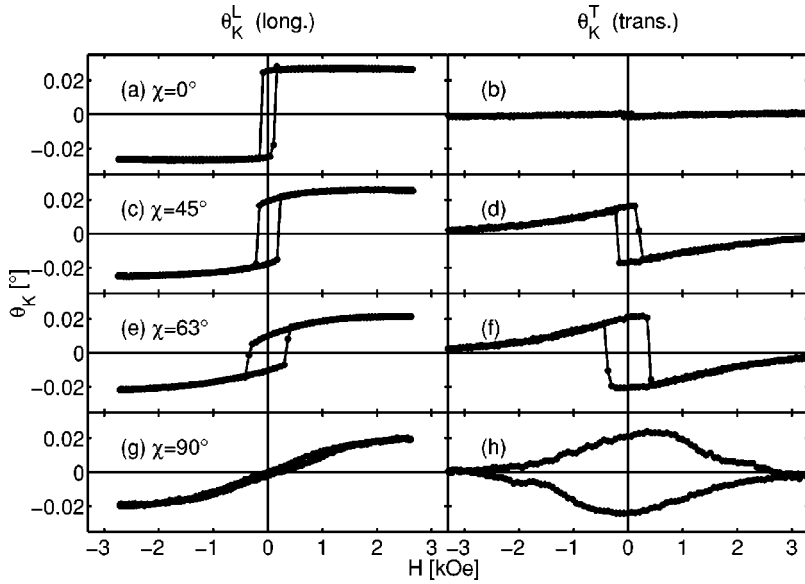


FIG. 4. MOKE hysteresis loops measured in the longitudinal configuration (left figures) and in the transverse configuration (right figures). For both configurations in (a) and (b), the external magnetic field is oriented parallel to the stripes (easy axis configuration); in (c) and (d), the stripes are rotated by 45° and in (e) and (f) by 63° with respect to the direction of the external field; in (g) and (h), the magnetic field is oriented perpendicular to the stripes (hard axis configuration).

same intensities for both spin-flip cross sections $(+, -)$ and $(-, +)$, the measurements can be reduced to only one spin-flip cross section. In this case, S'_a can be calculated from

$$S'_a = \frac{\sqrt{I_{+,+} + I_{+,-}} - \sqrt{I_{-,-} + I_{-,+}}}{\sqrt{I_{+,+} + I_{+,-}} + \sqrt{I_{-,-} + I_{-,+}}}. \quad (7)$$

From the $I(H)$ intensity values of the three cross sections $(+, +)$, $(-, -)$, and $(+, -)$, a magnetization curve can be calculated, which is proportional to the field-dependent magnetization of the stripes. The obtained curves may then be compared to the respective longitudinal MOKE hysteresis loops, after both have been normalized to their respective saturation magnetization.

In the case of nanostructured samples, the peak pattern in the off-specular scattering q_x direction depends on the angle between the stripes with respect to the scattering plane (see Fig. 3). Measurements at various angles of the stripe orientation are possible due to a poor resolution in q_y compared to a high resolution in q_x .^{20,31} Here q_x and q_y are the components of the scattering vector parallel and perpendicular to the scattering plane, respectively, and perpendicular to q_z , which is parallel to the film normal. By rotating the stripe pattern we are sensitive to the projection of their lattice parameter d into the scattering plane. For a sample rotation angle χ (see Fig. 3), the q_x component of the Bragg peak is therefore expected to occur at

$$q_x = \frac{2\pi \cos \chi}{d}. \quad (8)$$

By rotating the sample from the perpendicular orientation of the stripes to the scattering plane at $\chi=0^\circ$ towards a horizontal orientation, the q_x values decrease while the peak intensity strongly increases.

III. EXPERIMENTAL RESULTS

A. Results from MOKE measurements

The left row of Fig. 4 shows four typical longitudinal MOKE hysteresis loops taken from the CoFe stripes with different in-plane angles χ . The hysteresis loop in (a) corresponds to an external magnetic-field oriented parallel to the stripes. In this case, we find an almost square hysteresis loop, which represents the typical behavior of a sample when magnetically saturated along an easy axis of the magnetization. The coercive field is $H_c = 140$ Oe. The coercive field increases to $H_c = 200$ Oe and $H_c = 320$ Oe for intermediate angles of rotation of 45° (c) and 63° (e), respectively. Figure 4(g) shows the corresponding hysteresis loop for the CoFe stripe array oriented perpendicular to both the external field and the plane of incidence. Here, a typical hard axis hysteresis loop is obtained.

From the results of longitudinal MOKE measurements with the magnetic-field direction within the plane of incidence, we may indeed conclude that patterning of the thin CoFe film into an array of stripes induces a strong uniaxial anisotropy, which results from the shape anisotropy of CoFe stripes. The saturation field measured with MOKE along the hard axis is rather high, exceeding 1000 Oe.

As discussed above, we also determined the transverse component of the magnetization vector by Kerr effect measurements. Corresponding hysteresis loops for four directions of the external magnetic field relative to the direction of the CoFe stripes are shown in the right column of Fig. 4. The hysteresis loop reproduced in Fig. 4(b) was measured with a magnetic field parallel to the CoFe stripes, i.e., parallel to the easy axis. Ideally, within this configuration the measured Kerr rotation should remain zero unless components of the magnetization lie in the plane of incidence during the magnetization reversal process. As can be seen from Fig. 4(b), the measured Kerr rotation is indeed almost zero, thus no rotation of the magnetization occurs in this configuration. Figures 4(d) and 4(f) show the transverse component of the

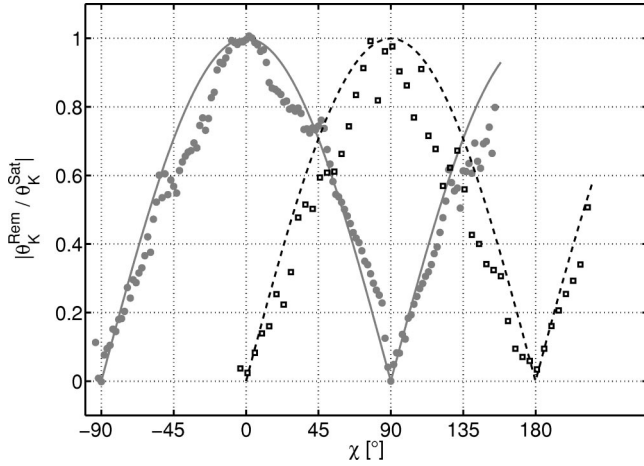


FIG. 5. Kerr rotation in remanence θ_K^{Rem} normalized to the saturation Kerr rotation θ_K^{Sat} as a function of the sample rotation. The closed circles are the measurements in the longitudinal configuration and the open squares denote the measurements in the perpendicular configuration. The solid line is a plot of the model according to Eq. (9) and the dashed line is a plot of Eq. (10).

Kerr rotation measured for angles of rotation of $\chi = 45^\circ$ and $\chi = 63^\circ$, respectively. Figure 4(h) shows the hysteresis loop for a magnetic field pointing along the hard axis direction, i.e., in a direction perpendicular to the stripes and the plane of incidence. In these directions, the measurements of the transverse magnetization component always proves a rotation of the magnetization away from the magnetic field.

From these measurements, important conclusion concerning the remagnetization process of the CoFe stripes can be drawn. In general, two ideal cases can easily be distinguished: If the angle of the magnetization vector changes without changing the magnitude $|M|$, then the magnetization reversal occurs via coherent rotation. On the other hand, if the angle of the magnetization vector remains constant within a certain magnetic-field range but the magnitude $|M|$ changes, then magnetic domains are formed. The hysteresis curves in Fig. 4 exhibit no discontinuity besides the jump at H_c , therefore the magnetization process must be smooth, either dominated by rotation or by domain nucleation. If only coherent rotation takes place, the magnetization in remanence must be directed along the easy axis of the twofold anisotropy, i.e., along the stripes, without forming any domains. In this case, the longitudinal Kerr rotation in remanence θ_K^{Rem} must follow:

$$\frac{\theta_K^{Rem,L}}{\theta_K^{Sat}} = |\cos \chi|, \quad (9)$$

and, correspondingly, the Kerr rotation angle in perpendicular configuration must follow

$$\frac{\theta_K^{Rem,T}}{\theta_K^{Sat}} = |\sin \chi|. \quad (10)$$

The measurements perfectly obey these rules as is depicted in Fig. 5. Therefore, it is clear that the magnetization process

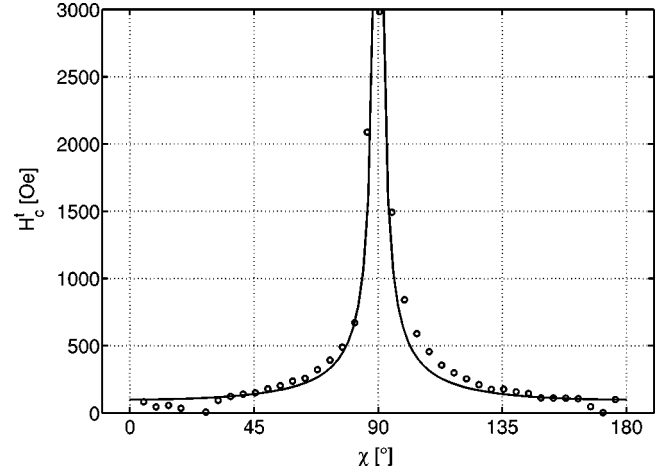


FIG. 6. Coercive field taken from the measurements in the perpendicular geometry as a function of the sample rotation χ . The circles denote the measurement and the solid line is a plot of Eq. (11).

is governed by coherent rotation processes. Furthermore, the coercive field should also show such a simple behavior: Along the easy axis, the magnetization switches by 180° if the external field is equal to the pinning field of the domains. If the sample is rotated away from the easy axis, the component of the external field driving the switching process is reduced. Therefore one finds

$$H_c(\chi) = \frac{H_c^{e.a.}}{\cos \chi}, \quad (11)$$

which is plotted in Fig. 6. Clearly the plot confirms this notion.

In summary, for fields parallel to the stripes the remagnetization process proceeds by nucleation and domain wall motion within a very narrow region around the coercive field H_c . For field directions $0 < \chi < 90^\circ$, the remagnetization process is dominated by a coherent rotation up to the coercive field, where some domains are formed. For $\chi = 90^\circ$, the remagnetization process appears to proceed entirely via a coherent rotation of the magnetization vector and no switching takes place. In the hard axis direction, the magnetization vector describes a complete 360° rotation during the full magnetization cycle without any discontinuity. For other directions, a switching of the magnetization of 180° is observed at H_c ; which can be viewed as a head-to-head domain wall movement³² through the stripe. Similar dependencies were found in Ref. 33, where the switching process was found to be dominated by edge curling walls.

Reason for this clear and straightforward remagnetization process is the high aspect ratio of the stripes (width/height = 13.3), leading to a strong shape anisotropy. The shape anisotropy results in a twofold anisotropy with an anisotropy energy density E_s . From a numerical integration of the magnetization curve in the hard axis direction follows $E_s \approx 730M_s$ Oe, where M_s is the saturation magnetization of the CoFe alloy. The energy density of the shape anisotropy can be calculated according to Ref. 15, using the relation

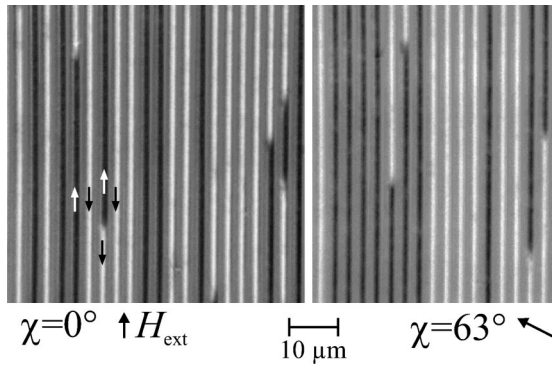


FIG. 7. Kerr-microscopy pictures taken around H_c for different magnetic field to sample alignment of $\chi=0^\circ$ (left, easy axis alignment) and $\chi=63^\circ$ (right). The plane of incidence results in a top-down magneto-optical sensitivity axis parallel to the stripes. The magnetization directions are indicated by arrows in the $\chi=0^\circ$ map.

$E_s = 2\pi N M_s^2$, where N is the tensor element of the demagnetizing tensor in the appropriate direction. N can be calculated as an approximation for an ellipsoid inscribed in the wire by using a formula given in Ref. 15. Assuming $M_s = 1775$ G for $\text{Co}_{0.7}\text{Fe}_{0.3}$, the theoretical shape anisotropy constant is 780 Oe M_s , which is in good agreement with our measurements. The value of the saturation magnetization M_s for $\text{Co}_{0.7}\text{Fe}_{0.3}$ is higher than the value for pure Fe and is given in Ref. 34 and references therein. More recent experiments confirm this value.³⁵

B. Results from Kerr microscopy

The Kerr-microscopy studies support the conclusions from the MOKE measurements. Images at different magnetic fields show a single domain state for a field below and above H_c (not shown). Around H_c , domain nucleation and domain wall movement sets in. The proposed mechanism of head-to-head domain walls through the stripes can be confirmed. From our observations, we assume independent domain nucleation and domain-wall movement for each single stripe. Possible existence of dipole-dipole interactions between domains of adjacent stripes cannot be extracted from the Kerr-microscopy observations in Fig. 7, which shows the Kerr-microscopy pictures taken at H_c for two different field angles χ of the sample rotation. In Fig. 7 (left), we show the easy axis case with no magnetization rotation for $H \neq H_c$, and in Fig. 7 (right), we show a picture taken from an intermediate angle $\chi=63^\circ$ close to the hard axis case. This angle was chosen for comparison with our neutron-scattering measurements, to be discussed later in the following section. In agreement with the MOKE results, at H_c , similar Kerr-microscopy pictures were found for different angles χ of the sample rotation between $\chi=0^\circ$ and $\chi=88^\circ$.

C. Results from neutron-scattering experiments

To optimize the experimental conditions for scanning the first-order Bragg peak of the stripe array as a function of the stripe orientation (Fig. 8), we have mapped out the position of the first-order Bragg peak as a function of the sample

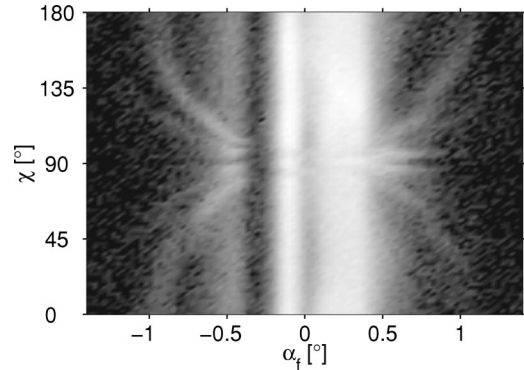


FIG. 8. Results of an unpolarized neutron-scattering measurement. The intensity was measured with a position sensitive detector as a function of the sample rotation χ and the angle of the final neutron beam α_f . The gray-scale intensity in the figure is proportional to the logarithmic neutron counts. The measurements were performed between a perpendicular orientation of the stripes with respect to the scattering plane ($\chi=0^\circ$) over an 180° angle range to again a perpendicular orientation at $\chi=+180^\circ$. The angle of the initial beam α_i was fixed to $\alpha_i=0.32^\circ$. The “X” in the pattern corresponds to the first order Bragg peak of the wire array. The vertical line in the middle of the pattern is from the specular beam, the left line comes from the partly blocked direct beam.

rotation. The corresponding map is shown in Fig. 8. The angle of the incident unpolarized neutron beam α_i was fixed to the angle of total external reflection $\alpha_i = \alpha_c = 0.31$, and the intensity was measured as a function of the angle of the exit neutron beam α_f for sample rotations χ between $0^\circ \leq \chi \leq 180^\circ$ using a position sensitive detector (PSD). A first-order Bragg peak occurs for all sample rotations, even for $\chi=0^\circ$ and $\chi=180^\circ$ where the peaks are very weak. However, in sample configurations with angles χ close to the hard axis (at $\chi=90^\circ$), the first-order Bragg peak moves very close to the ridge of specular reflection and an additional second-order Bragg peak appears. In Fig. 8, Bragg reflections become also visible from the back side of the sample.

Next, we explore the reciprocal space for a fixed χ angle by taking off-specular intensity maps with polarized neutrons. The results are plotted in $q_z - q_x$ maps. In Fig. 9, typical maps are shown that were taken with spin-up polarized neutrons (top panel) and with spin-down polarized neutrons (bottom panel) at a sample rotation of $\chi=45^\circ$. The specular beam does not exhibit finite-size oscillations, probably due to the artificial “roughness” of the sample. As a result, no splitting between spin-up and spin-down specular reflectivities can be observed. In the off-specular regime, Bragg peaks of the first and second order from the stripe array can be recognized. The highest intensity is from the first-order reflections. Their intensity is enhanced due to a resonance amplification from the Yoneda wings, on which they are positioned.³⁶ The Bragg peaks show a strong intensity difference for spin-up and spin-down polarized neutrons and therefore carry magnetic information. Below the sample horizon the transmitted direct beams from the front- and back-side measurements are visible as well.

We have carried out magnetization reversal measurements for different sample rotation angles χ by measuring the intensities from the different cross sections at the first-order

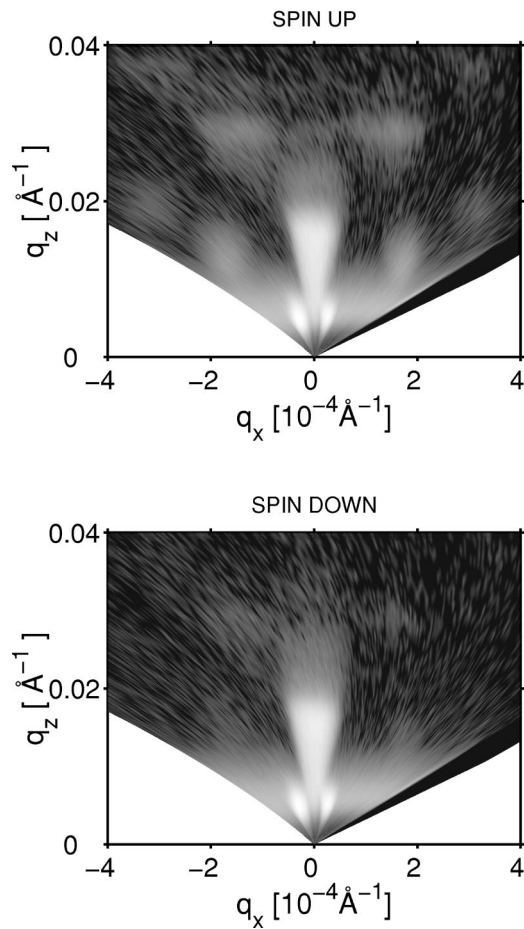


FIG. 9. Results of a polarized neutron-scattering measurement. The intensity was measured via PSD as function of q_x and q_z . The sample rotation was fixed to $\chi=45^\circ$. The left pattern was taken with spin-up neutrons, and the right pattern with spin-down neutrons. The gray-scale intensity in the figure is proportional to the logarithmic neutron counts.

Bragg peak (see above). For $\chi=0^\circ$ (easy axis configuration), the scans are taken at $\alpha_i=0.32^\circ$ and $\alpha_f=1.06^\circ$ (Fig. 10, top panels). For the other χ angles ($\chi=45^\circ$ in the middle panels and $\alpha_f=0.62^\circ$ in the bottom panels), only the α_f value had to be readjusted for maximum intensity, while the α_i value was kept constant. For higher χ values than $\chi=63^\circ$, the first-order Bragg peak position moves too close to the specular ridge to be resolved.

The left column of panels of Fig. 10 show hysteresis measurements performed at the first-order Bragg peak via polarized neutron scattering. From these measurements, the neutron-derived magnetic hysteresis can be evaluated and compared to hysteresis loops determined by magneto-optical MOKE measurements (right column of graphs of Fig. 10). The measurements were performed between 0 Oe and 800 Oe and between 720 Oe and 0 Oe (see above). In Fig. 10, the second part of the measurements is plotted as a part of the hystereses between -720 Oe and 0 Oe, which is an allowed procedure for symmetry reasons.

The top panel in Fig. 10 for $\chi=0^\circ$ exhibits a large splitting of the $(+, +)$ and $(-, -)$ intensities, which reverses

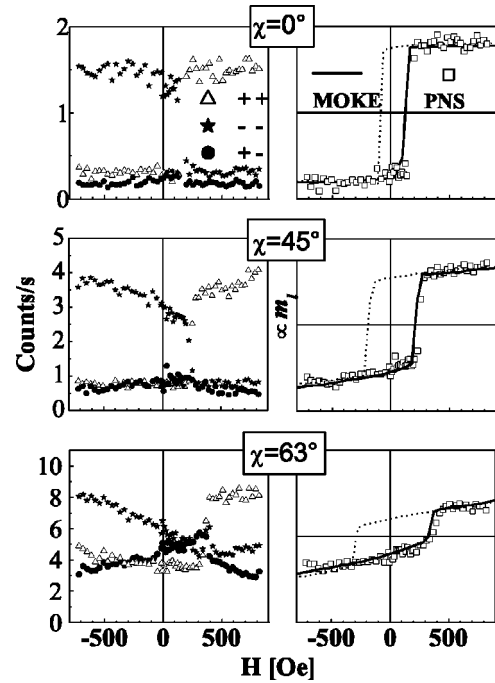


FIG. 10. Magnetization reversal measurements performed at the first-order Bragg peak for three different cross sections (left column) and calculated curves from the polarized neutron measurements (right column). The calculated curves are compared to longitudinal MOKE hysteresis loops, reproduced as solid and dotted lines. The top row depicts measurements at a sample rotation of $\chi=0^\circ$, the middle row measurements at a sample rotation of $\chi=45^\circ$, and the bottom row measurements at a sample rotation of $\chi=63^\circ$.

suddenly at the coercive field H_c . There is almost no spin-flip scattering visible over the entire field range, indicating that the magnetization reversal for the easy axis configuration takes place in the form of nucleation and fast domain-wall movements at H_c , in complete agreement with the conclusions from the MOKE measurements.

At $\chi=45^\circ$, the $(+, +) - (-, -)$ splitting starts to become reduced for field values far above and below H_c , while the spin-flip scattering shows a gentle slope towards the coercive field. The corresponding MOKE results shown in Fig. 4 are consistent with a coherent rotation model. The neutron cross sections qualitatively confirm this notion in all details. Quantitatively, there may indeed be a difference between the average angle for coherent magnetization rotation and its first Fourier component measured by PNS. In fact, we observe at the specular ridge more spin-flip scattering than in the first-order Bragg peak, in agreement with the MOKE results.

The situation is more pronounced for the sample rotation of $\chi=63^\circ$. The $(-, -)$ intensity continuously decreases with increasing field from negative to positive field values, while the $(+, +)$ intensity is more or less constant for most of the field values and changes suddenly at the coercive field. At the same time, the spin-flip intensity increases again towards the coercive field, however, with a larger slope. All four cross sections are again consistent with a coherent rota-

tion of the magnetization vector away from the easy axis, in very good agreement with the conclusions from our MOKE measurements.

The situation changes at H_c where 180° head-to-head domains are created in the individual stripes and domain-wall movement sets in. A single domain state again is reached for fields slightly larger than H_c . In our neutron-scattering experiment, the field range in which domain nucleation and domain-wall movement occur, is presented by only few data points and therefore, the general behavior is dominated by a single domain state with a constant or a rotating magnetization.

More quantitative statements can be made by evaluating the spin asymmetry related expression S'_a (see above), using the $I(H)$ intensities of the cross sections $(+, +)$, $(-, -)$, and $(+, -)$. The neutron hysteresis curves (open squares) are compared to the respective longitudinal MOKE hysteresis loops (solid and dotted lines) for the same sample rotation, as shown in the bottom graphs of Fig. 10. The overall agreement is rather good for all three sample rotation angles.

IV. DISCUSSION

If the remagnetization process does not involve a complicated domain structure, in general, good agreement can be expected between polarized neutron reflectivity and results from other methods. This has been demonstrated for homogeneous magnetic films by a number of investigators.^{23–25} In our case, the agreement has to be reestablished. First, the sample is not homogeneous but laterally structured, and second, we compare off-specular neutron Bragg reflections with specular vector MOKE and with MOKE microscopy. Nevertheless, the main conclusions from the MOKE measurements could be confirmed by PNS. Those are given as follows.

(i) Only for $\chi=0^\circ$ the orientation of the magnetization is constant for all field values and parallel to the magnetic stripes. At $H=H_c$ nucleation and domain wall motion occurs.

(ii) Independent of the sample rotation angle and for magnetic fields below the coercive field H_c , a single domain state is present.

(iii) For rotation angles $\chi>0^\circ$ below H_c , a coherent spin rotation occurs with increasing field away from the easy axis.

(iv) For a rotation angle of $\chi\sim 90^\circ$, the remagnetization process consists solely of a coherent magnetization rotation without nucleation.

The good agreement between both the methods is a result of the single domain state, which is present for all rotation angles and for all field values different from the coercive field. Furthermore, the interactions and correlation effects appear to be negligible. This simple domain structure, which follows from the sample design, furnishes a good testing ground for comparative studies. As the domain state becomes more complex and correlation effects are present, we expect deviations between the MOKE and the PNS results.

Deviations between hysteresis measurements taken at the specular reflected beam and higher-order diffracted beams have been observed with MOKE at several magnetic microstructures, as was reported, e.g., in Refs. 14,37,38 (and ref-

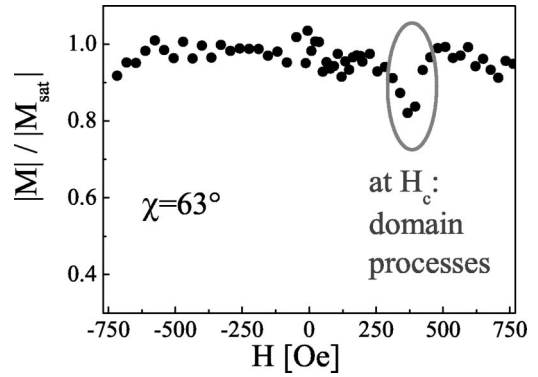


FIG. 11. Results for $|M/M_{sat}|$ at the $\chi=63^\circ$ orientation. The normalized magnetization was derived from the non-spin-flip and the spin-flip Bragg intensities.

erences therein). In these studies, it was observed that the diffracted beam of order n is proportional to the n th-order Fourier component of the magnetization distribution of the stripes. Therefore, one should expect equivalent effects for PNS for $n\neq 0$, if domains are present in the stripes, which will be explored in more detail in the future.

So far our discussion was concentrated on domain rotation. However, neutron scattering can also provide information on the nucleation process. Combining results from the spin-flip and the non-spin-flip cross sections allows to derive values for the angle and the length of the magnetization vector \vec{M} , similar to vector MOKE. As a constant length of the magnetization vector accounts for rotational processes and a changing length for domain nucleation and domain-wall movement, we calculated $|M/M_{sat}|$ for the $\chi=63^\circ$ configuration with the highest spin-flip intensities observed. The result is shown in Fig. 11.

Since the magnetization reversal is dominated by a coherent rotation of the magnetization vector, the magnitude of \vec{M} does not change over most of the field range. In this respect, the neutron results perfectly agree with our MOKE data for most of the field range, as mentioned before. A small dip occurs, however, at H_c . This is due to domain nucleation and domain-wall movement within this small field range.

From the present neutron-scattering experiments on a magnetic stripe array several conclusions can be drawn, which are important for future studies and for the potential of this method in general. First, several orders of Bragg peaks in the off-specular scattering regime can be recognized in measurements with unpolarized (Fig. 8) and polarized neutrons (Fig. 9). By rotating the stripes with respect to the scattering plane, the peak position q_x changes because the effective period changes according to Eq. (8). Samples with a pattern period of about $3\ \mu\text{m}$ are ideally suited for scattering experiments in the off-specular regime. For smaller periods, the intensity of the first-order Bragg peak becomes too small, and for larger periods, the Bragg peaks move too close to the specular ridge to be well enough separated. Periods of about $3\ \mu\text{m}$ are an ideal compromise. In this case, a first-order Bragg peak can be identified over the complete sample rotation range. Only for small angles, the first-order peak moves very close to the position of the specular scattering

and can no longer be resolved.

V. SUMMARY

We have studied the magnetization reversal behavior of a $\text{Co}_{0.7}\text{Fe}_{0.3}$ stripe array with a grating period of $3\mu\text{m}$, which was generated by scanning laser lithography. Using polarized neutron scattering (PNS), vector MOKE, and Kerr microscopy, we have analyzed and compared the magnetic hysteresis as a function of angle χ between the stripes and the applied field.

The MOKE experiments were carried out with the field parallel to the scattering plane (longitudinal configuration) and perpendicular to the scattering plane (transverse configuration). The combination of this yields both components of the in-plane magnetization vector. Similarly, we have investigated the magnetic hysteresis of the same sample with polarized neutron scattering at small angles using the first-order Bragg peak from the stripe array in the off-specular q_x direction. Unlike the MOKE experiment, for the polarized neutron-scattering experiment, the magnetic field is always applied perpendicular to the scattering plane and parallel to the polarization axis of the neutrons. Both components of the in-plane magnetization then follow from an analysis of the non-spin-flip $[(+,+),(-,-)]$ and spin-flip $[(+,-),(-,+)]$ cross sections.

The results from vector MOKE and from PNS agree very well. Both the methods confirm that for most of the field values the stripes are in a single domain state. In case that the field is applied parallel to the stripe axis (easy axis), a domain nucleation and a domain-wall movement occurs within a narrow field range at the coercive field. For all other

sample orientations we observe a coherent magnetization rotation with increasing field with some domain nucleation occurring just around H_c . However, for a stripe orientation perpendicular to the applied field, the domain rotation is complete without nucleation processes.

The good agreement between MOKE and PNS is in part due to the sample design providing a large uniaxial anisotropy and in part due to the lack of interaction among the stripes. This provides confidence for more complex situations to be studied in the future. In particular, for domain formation and correlation effects, investigations at Bragg reflections with polarized neutrons will filter out the respective Fourier components of the remagnetization process.

It should be mentioned here that most recently the magnetic order in a Co/Pt line array with perpendicular anisotropy has been investigated via the x-ray magnetic scattering (XRMS) technique by Chesnel *et al.*³⁹ In the demagnetized state the authors find an antiferromagnetic dipolar coupling between the stripes leading to an antiferromagnetic order with a mean correlation length of about four lines. Both techniques, XRMS and PNS will play a crucial role in the future, when it comes to the analysis of magnetic correlation lengths and phase transitions in nanostructured magnetic gratings. We are just at the beginning of this new research field.

ACKNOWLEDGMENTS

The authors would like to thank Axel Carl, Günter Reiss, and Boris Toperverg for fruitful discussions. We acknowledge funding by the SFB 491 "Magnetic heterostructures and electronic transport" and by the BMBF under contract O3ZAE8BO.

*Electronic address: k.theis-broehl@ruhr-uni-bochum.de URL: <http://www.ep4.ruhr-uni-bochum.de>

¹J.I. Martín, M. Vélez, J. Nogués, and I.K. Schuller, Phys. Rev. Lett. **79**, 1929 (1997).

²Y. Jaccard, J.I. Martín, M.-C. Cyrille, M. Vélez, J.L. Vicent, and I.K. Schuller, Phys. Rev. B **58**, 8232 (1998).

³D.J. Morgan and J.B. Ketterson, Phys. Rev. Lett. **80**, 3614 (1998).

⁴T. Shinjo, T. Okuno, R. Hassdorf, K. Shigeto, and T. Ono, Science (Washington, DC, U.S.) **289**, 1831 (2001).

⁵R.P. Cowburn, Phys. Rev. B **65**, 092409 (2002).

⁶Gang-Xiong, D.A. Allwood, M.D. Cooke, and R.P. Cowburn, Appl. Phys. Lett. **79**, 3461 (2001).

⁷T. Ono, Y. Ooka, S. Kasai, H. Miyajima, K. Mibu, and T. Shinjo, J. Magn. Magn. Mater. **226-230**, 930 (2001).

⁸H. Zhu, S. Yang, G. Ni, D. Yu, and Y. Du, J. Magn. Magn. Mater. **234**, 454 (2001).

⁹S. Yang, H. Zhu, D. Yu, Z. Jin, S. Tang, and Y. Du, J. Magn. Magn. Mater. **222**, 97 (2001).

¹⁰T. Schmitte, K. Theis-Bröhl, V. Leiner, H. Zabel, S. Kirsch, and A. Carl, J. Phys.: Condens. Matter **14**, 7525 (2002).

¹¹C. Shearwood, S.J. Blundell, M.J. Baird, J.A.C. Bland, M. Gester, and E. Ahmed, J. Appl. Phys. **75**, 5249 (1994).

¹²T. Schmitte, T. Schemberg, K. Westerholt, H. Zabel, K. Schädler, and U. Kunze, J. Appl. Phys. **87**, 5630 (2000).

¹³T. Schmitte, O. Schwöbken, S. Goek, K. Westerholt, and H. Za-

bel, J. Magn. Magn. Mater. **240**, 24 (2002).

¹⁴T. Schmitte, K. Westerholt, and H. Zabel, J. Appl. Phys. **92**, 4524 (2002).

¹⁵A. Hubert and R. Schäfer, *Magnetic Domains* (Springer, Heidelberg, 1998).

¹⁶H.P. Oepen and J. Kirschner, Scanning Microsc. **5**, 1 (1991).

¹⁷J.N. Chapman, A. Johnston, L.J. Heydermann, S. McVitie, W.A.P. Nicholson, and B. Bormans, IEEE Trans. Magn. **30**, 4479 (1994).

¹⁸P. Fischer, T. Eimuller, G. Schütz, G. Schmahl, P. Guttmann, and G. Bayreuther, J. Magn. Magn. Mater. **198**, 624 (1999).

¹⁹J. Schmidt, G. Skidmore, S. Foss, E. Dan Dahlberg, and C. Merton, J. Magn. Magn. Mater. **190**, 81 (1998).

²⁰B.P. Toperverg, G.P. Felcher, V.V. Metlushko, V. Leiner, R. Siebrecht, and O. Nikonov, Physica B **283**, 9395 (2000).

²¹K. Temst, M.J. Van-Bael, and H. Fritzsche, Appl. Phys. Lett. **79**, 991 (2001).

²²K. Temst, M.J. Van-Bael, V.V. Moshchalkov, Y. Bruynseraede, H. Fritzsche, and R. Jonckheere, Appl. Phys. A: Mater. Sci. Process. **A74**, S1538 (2002).

²³M.R. Fitzsimmons, P. Yashar, C. Leighton, Ivan K. Schuller, J. Nogués, C.F. Majkrzak, and J.A. Dura, Phys. Rev. Lett. **84**, 3986 (2000).

²⁴F. Radu, M. Etzkorn, R. Siebrecht, T. Schmitte, K. Westerholt, and H. Zabel, Phys. Rev. B **67**, 134409 (2003).

- ²⁵F. Radu, M. Etzkorn, T. Schmitte, R. Siebrecht, A. Schreyer, K. Westerholt, and H. Zabel, *J. Magn. Magn. Mater.* **240**, 251 (2002).
- ²⁶C. Daboo, R.J. Hicken, E. Gu, M. Gester, S.J. Gray, D.E.P. Eley, E. Ahmad, J.A.C. Bland, R. Ploessl, and J.N. Chapman, *Phys. Rev. B* **51**, 15 964 (1995).
- ²⁷H. Kikuchi, M. Sato, and K. Kobayashi, *J. Appl. Phys.* **87**, 6055 (2000).
- ²⁸H. Brückl, J. Schmalhorst, H. Boeve, G. Gieres, and J. Wecker, *J. Appl. Phys.* **91**, 7029 (2002).
- ²⁹Th. Zeidler, F. Schreiber, H. Zabel, W. Donner, and N. Metoki, *Phys. Rev. B* **53**, 3256 (1996).
- ³⁰F. Schmidt, W. Rave, and A. Hubert, *IEEE Trans. Magn.* **21**, 1596 (1985).
- ³¹B. Dorner and A. Wildes, *Langmuir* (to be published).
- ³²P.D. McMichael and M.J. Donahue, *IEEE Trans. Magn.* **33**, 4167 (1997).
- ³³R. Mattheis, K. Ramstöck, and J. McCord, *IEEE Trans. Magn.* **33**, 3993 (1997).
- ³⁴R. M. Bozorth, *Ferromagnetism* (D. van Nostrand Company, Princeton, 1968), p. 194, Chap. 6, Figs. 6-4.
- ³⁵E.J. Yun, W. Win, and R.M. Walser, *IEEE Trans. Magn.* **32**, 4535 (1996).
- ³⁶H. Dosch, *Critical Phenomena at Surfaces and Interfaces*, Springer Tracts in Modern Physics Vol. 126 (Springer, Heidelberg, 1992).
- ³⁷O. Geoffroy, D. Givord, Y. Otani, B. Pannetier, A.D. Santos, M. Schlenker, and Y. Souche, *J. Magn. Magn. Mater.* **121**, 516 (1995).
- ³⁸I. Guedes, N.J. Zaluzec, M. Grimsditch, C. Metlushko, P. Vavasori, B. Ilic, P. Neuzil, and R. Kumar, *Phys. Rev. B* **62**, 11 719 (2000).
- ³⁹K. Chesnel, M. Belakhovsky, S. Landis, J.C. Toussaint, S.P. Collins, G. van der Laan, E. Dudzik, and S.S. Dhesi, *Phys. Rev. B* **66**, 024435 (2002).